Electrical control of intrinsic nonlinear Hall effect in antiferromagnetic topological insulator sandwiches

Ruobing Mei,[1] Daniel Kaplan,[2] Binghai Yan,[3] Cui-Zu Chang,[1] and Chao-Xing Liu[1,*]

[1]*Department of Physics, The Pennsylvania State University, University Park, Pennsylvania 16802, USA*

[2]*Center for Materials Theory, Department of Physics and Astronomy, Rutgers University, Piscataway, New Jersey 08854, USA*

[3]*Department of Condensed Matter Physics, Weizmann Institute of Science, Rehovot 7610001, Israel*

(Received 3 July 2024; accepted 12 September 2024; published 1 October 2024)

A nonlinear Hall effect (NHE) can originate from the quantum metric mechanism in antiferromagnetic topological materials with PT symmetry, which has been experimentally observed in $MnBi_2Te_4$. In this paper, we propose that breaking PT symmetry via external electric fields can lead to a dramatic enhancement of NHE, thus allowing for an electric control of NHE. Microscopically, this is because breaking PT symmetry can lift the spin degeneracy of a Kramers pair, giving rise to additional contributions within one Kramers pair of bands. We demonstrate this enhancement through a model Hamiltonian that describes an antiferromagnetic topological insulator sandwich structure.

DOI: 10.1103/PhysRevB.110.165401

I. INTRODUCTION

Integrating magnetism into topological insulators (TIs) can break time reversal (T) symmetry and lead to the emergence of magnetic topological phases, e.g., quantum anomalous Hall (QAH) insulators [1–8] and axion insulators (AIs) [9–12]. Magnetism has been successfully achieved in TIs by either doping magnetic impurities, e.g., Cr- and/or V-doped $(Bi, Sb)_2Te_3$, or growing a stoichiometric antiferromagnetic topological compound, $MnBi_2Te_4$. When ferromagnetism is achieved in TI films, both surface states are gapped, leading to the QAH effect [1,8,13,14]. The quantized Hall response for QAH states has been unambiguously observed in several systems, including magnetically doped TIs [3–6], $MnBi_2Te_4$ films [7], and twisted graphene and transition metal dichalcogenide materials [15–24]. When two surface states of TI films are gapped by antiferromagnetic (AFM) alignment of magnetization, which can be achieved in a magnetic TI sandwich structure with AFM alignment at two surfaces (dubbed as "AFM TIs" below), as shown in Fig. 1(a), or in even septuple layers (SLs) of $MnBi_2Te_4$ films [25,26], the AI phase was theoretically predicted and can host a quantized magnetoelectric response [10,27–29]. A zero Hall plateau observed in these AFM TIs [11,12] provides evidence for the AI phase. Optical experiments have also been studied in AFM TIs to explore the axion electrodynamics of the AI phase [30–34].

Recently, quantized topological and nonquantized geometric responses have been generalized to the nonlinear regime in topological materials [35–44]. A notable example is the nonlinear Hall effect (NHE), which describes the Hall current response at the nonlinear order of electric fields. There are two major intrinsic geometric mechanisms for NHE, the Berry curvature dipole [45–48] and the quantum metric dipole [49–52]. These two mechanisms have different symmetry properties. The Berry curvature dipole-induced NHE can exist in a T-symmetric system, but is forbidden by PT symmetry, where P is inversion. This is because PT symmetry guarantees the double degeneracy of all bands at each momentum. Due to its similarity to Kramers' theorem for T-symmetric systems [53,54], these spin degenerate bands are dubbed "Kramers pairs" below. As a result, the Berry curvature, as well as the Berry curvature dipole, has to vanish at each momentum in the Brillouin zone (BZ). In contrast, the quantum metric dipole (also called "intrinsic NHE" [49,52]) requires the T breaking, but it can exist in a PT-symmetric system. The AFM TIs can possess PT symmetry but break both P and T symmetry due to the AFM order, and thus provide an ideal platform to examine the intrinsic NHE induced by a quantum metric. Recently, intrinsic NHE has been experimentally observed in even SLs of $MnBi_2Te_4$ films [55,56]. The quantum metric mechanism requires breaking both T and P but also occurs in PT-breaking systems. Our main objective is to understand the dependence of intrinsic NHE on the PT breaking, achieved by an out-of-plane electric field.

In this paper, we study the NHE in a model Hamiltonian of AFM TIs under electric fields in Figs. 1(a) and 1(b). Inversion symmetry breaking by electric fields can lift the spin degeneracy of a Kramers pair of bands. Although these two spin bands are no longer degenerate in energy, we continue using the terminology "Kramers pair" to denote them. In PT-symmetric systems, only the contribution between different Kramers pairs of bands (dubbed "inter-Kramers pairs" below) exist for the NHE. Our main result here is to show additional NHE contributions from two spin bands within one Kramers pair (dubbed "intra-Kramers pair" below) can emerge when the inversion symmetry breaking is strong enough so that the energy splitting between the two spin bands is larger than disorder broadening. Furthermore, we find the intra-Kramers-pair NHE contribution can dominate over the inter-Kramers-pairs

*Contact author: cxl56@psu.edu

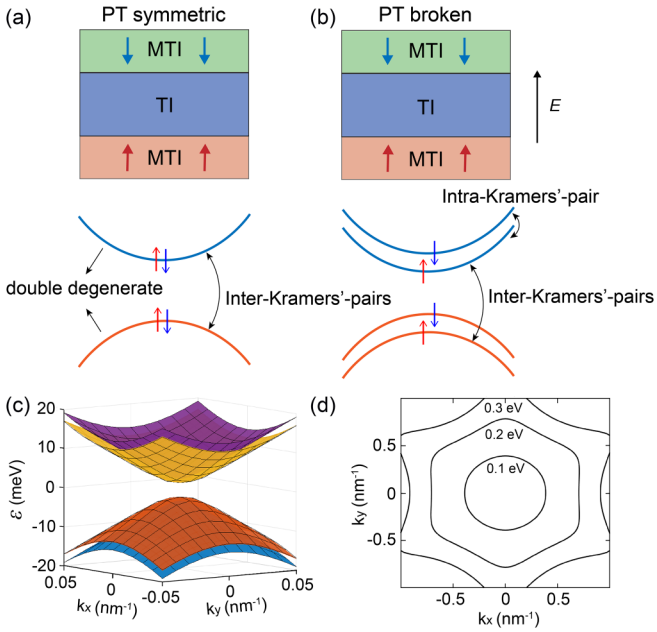

FIG. 1. (a) PT-symmetric magnetic TI sandwich structure. Each band is doubly degenerate due to the PT symmetry and the quantum metric dipole only arises between different Kramers pairs of bands. (b) When an external electric field breaks PT symmetry, the Kramers pairs split in energy, giving rise to additional contributions between two bands within one Kramers pair. (c) The energy dispersion for $t = 2$ meV and $V_0 = 1$ meV. (d) Fermi-surface contours of the lowest conduction band at the Fermi energies $\varepsilon_f = 0.1$, 0.2, and 0.3 eV.

NHE contribution in the thin-film limit when the top and bottom surface states are strongly hybridized. We predict an enhancement of the intrinsic NHE in AFM TIs due to the PT-symmetry breaking.

II. MODEL HAMILTONIAN AND SYMMETRY FOR AFM TIs

We consider a model Hamiltonian for the AFM TI sandwiches, as shown in Fig. 1(a), where the top and bottom surface states open the gaps with opposite signs. We assume the Fermi energy is within the TI bulk, so the low-energy effective Hamiltonian for two surface states reads

$$H = v_f(k_y\sigma_x - k_x\sigma_y)\tau_z + m\sigma_z\tau_z + \lambda(k_+^3 + k_-^3)\sigma_z\tau_z + t\tau_x + V_0\tau_z, \quad (1)$$

where σ_i and τ_i $(i = x, y, z)$ are Pauli matrices in the spin and surface states basis, v_f is the Fermi velocity, m is the exchange coupling strength, λ is the hexagonal warping coefficient [57], and $k_\pm = k_x \pm ik_y$. We choose the parameters to be $v_f = 2.55\,\text{eV Å}$, $\lambda = 125\,\text{eVÅ}^3$, and $m = 1$ meV [57]. V_0 is the asymmetric potential created by the out-of-plane electric field E, $V_0 = eEd$, where d is the TI film thickness. The coupling parameter t describes the hybridization strength between the top and bottom surface states, which quickly decays as the film thickness d increases and is chosen in the range of 0–10 meV [58–61].

The model Hamiltonian breaks $P = \tau_x$ and $T = i\sigma_y K$ symmetries, and preserves $C_{3z} = e^{-i\frac{\pi}{3}\sigma_z}$ and $M_x T = -i\sigma_z K$ symmetries. In particular, the exchange coupling term breaks P, T, $M_x = i\sigma_x$, and $M_y = i\sigma_y$ symmetries, the hexagonal warping term breaks the full rotational symmetries down to the C_{3z} symmetry, and the asymmetric potential term V_0 breaks P and PT symmetries. When the asymmetric potential is absent, the system is PT symmetric. The symmetry properties of this system also give a strong constraint on the form of nonlinear conductivity σ_{abc}, defined by $j^a = \sigma_{abc}E^bE^c$, where $a, b, c = x, y$. From the symmetry analysis shown in the Supplemental Material [62] (see also Refs. [63–67] therein), $M_x T$ requires $\sigma_{yyy} = \sigma_{yxx} = \sigma_{xyx} = \sigma_{xxy} = 0$ while C_{3z} requires $\sigma_{xyy} = \sigma_{yxy} = \sigma_{yyx} = -\sigma_{xxx}$. Therefore, σ_{xyy} is the only independent component.

The eigenenergies of the Hamiltonian can be solved as $\varepsilon_{n\mu} = n\sqrt{t^2 + (A + \mu V_0)^2}$, where $n, \mu = \pm$ and $A = \sqrt{v_f^2k^2 + [m + 2\lambda k_x(k_x^2 - 3k_y^2)]^2}$, where n is the index for different sets of Kramers pairs and μ labels two spin states in one Kramers pair. When $V_0 = 0$, there are two sets of degenerate Kramers pairs with the eigenenergies $\varepsilon_\pm = \pm\sqrt{A^2 + t^2}$. Such degeneracy is broken by a nonzero V_0 in Fig. 1(c), where the energy dispersion is calculated for $t = 2$ meV and $V_0 = 1$ meV. Figure 1(d) depicts the Fermi-surface contours of the lowest conduction band at different energies, where the hexagonal warping effect is visible for a large momentum k.

III. QUANTUM-METRIC-INDUCED NHE IN PT-SYMMETRIC AND PT-BREAKING SYSTEMS

Since the Berry curvature dipole is forbidden by C_{3z} [45,68], it is excluded in our model even when PT symmetry is broken. Therefore, we focus on the intrinsic NHE. The intrinsic nonlinear Hall conductivity can be written as (see Supplemental Material [62])

$$\sigma_{xyy} = -\frac{e^3}{\hbar}\sum_{n\mu,m\nu}\int\frac{d^3k}{(2\pi)^3}f_{n\mu}\big[\partial_x\big(\alpha_{n\mu,m\nu}g^{yy}_{n\mu,m\nu}\big) + \partial_y\big(\beta_{n\mu,m\nu}g^{xy}_{n\mu,m\nu}\big)\big], \quad (2)$$

where $\partial_a = \frac{\partial}{\partial k_a}$ and $f_{n\mu} = \frac{1}{e^{(\varepsilon_{n\mu}-\varepsilon_f)/\Gamma}+1}$ is the Fermi distribution function, with the eigenenergy $\varepsilon_{n\mu}$, the Fermi energy ε_f, and the temperature broadening $\Gamma = k_BT$. The band-resolved quantum metric reads [50]

$$g^{ab}_{n\mu,m\nu} = \mathcal{A}^a_{n\mu,m\nu}\mathcal{A}^b_{m\nu,n\mu} + \mathcal{A}^b_{n\mu,m\nu}\mathcal{A}^a_{m\nu,n\mu}, \quad (3)$$

where $\mathcal{A}^a_{n\mu,m\nu} = \langle n\mu|i\partial_a|m\nu\rangle$ is the Berry connection, and $|n\mu\rangle$ is the eigenwave function of the Hamiltonian. The remaining dependence on disorder broadening $\Delta_\tau = \hbar/\tau$ with the relaxation time τ in the intrinsic conductivity is via the functions α and β, defined as

$$\alpha_{n\mu,m\nu} = \text{Re}\left[\frac{\varepsilon_{n\mu,m\nu}}{\Delta_\tau(i\varepsilon_{n\mu,m\nu} + \Delta_\tau)} - (n\mu \leftrightarrow m\nu)\right], \quad (4)$$

$$\beta_{n\mu,m\nu} = \text{Re}\left[\frac{\varepsilon_{n\mu,m\nu}}{i\varepsilon_{n\mu,m\nu} + \Delta_\tau/2}\left(\frac{1}{i\varepsilon_{n\mu,m\nu} + \Delta_\tau} + \frac{1}{\Delta_\tau}\right) - (n\mu \leftrightarrow m\nu)\right]. \quad (5)$$

This dependence becomes significant whenever the energy difference $\varepsilon_{n\mu,m\nu} = \varepsilon_{n\mu} - \varepsilon_{m\nu}$ is of the order of Δ_τ.

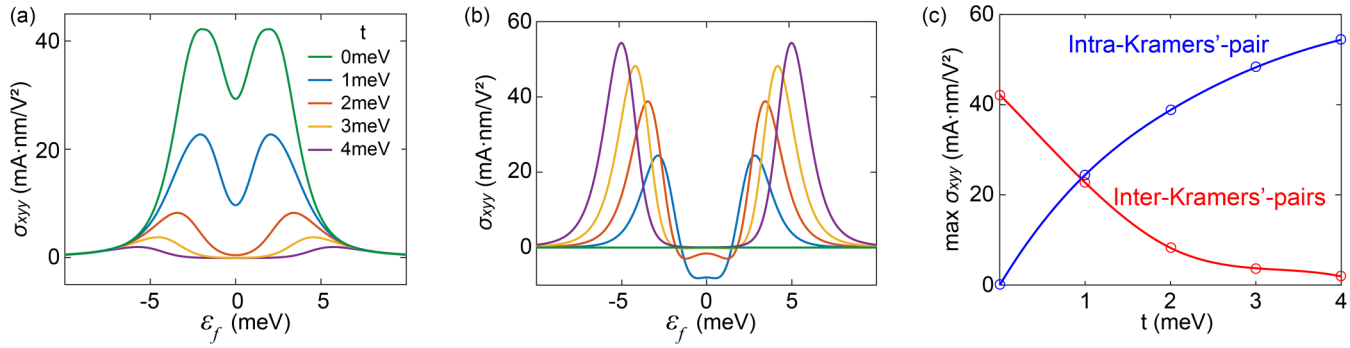

FIG. 2. (a) $\sigma_{xyy}^{\text{inter}}$ as a function of Fermi energy ε_f for the inter-Kramers-pairs contribution at $V_0 = 2\,\text{meV}$, $\Gamma = 0.6\,\text{meV}$, and $t = 0$, 1, 2, 3 and 4 meV. (b) $\sigma_{xyy}^{\text{intra}}$ as a function of Fermi energy ε_f for the intra-Kramers-pair contribution with different t. (c) The maximum value of $\sigma_{xyy}^{\text{inter}}$ and $\sigma_{xyy}^{\text{intra}}$ with respect to Fermi energy ε_f as a function of coupling coefficient t.

For the PT-symmetric case, the two spin bands within one Kramers pair ($n = m$) are degenerate so that $\varepsilon_{n\mu,n\nu} = 0$ and thus $\alpha_{n\mu,n\nu} = \beta_{n\mu,n\nu} = 0$. Therefore, the degenerate states within one Kramers pair give no contribution. We consider the case when the energy difference between different sets of Kramers pairs is much larger that the disorder level, i.e., $\varepsilon_{n\mu,m\nu} \gg \Delta_\tau$ ($n \neq m$), and can apply the expansion

$$\frac{1}{i\varepsilon_{n\mu,m\nu} + \Delta_\tau} = \frac{1}{i\varepsilon_{n\mu,m\nu}} + \frac{\Delta_\tau}{\varepsilon_{n\mu,m\nu}^2} + O\big(\Delta_\tau^2\big). \tag{6}$$

Up to the first order in Δ_τ, we find $\alpha_{n\mu,m\nu} = \frac{2}{\varepsilon_{n\mu,m\nu}}$ and $\beta_{n\mu,m\nu} = -\frac{1}{\varepsilon_{n\mu,m\nu}}$ for $n \neq m$, which leads to

$$\sigma_{xyy} = -\frac{e^3}{\hbar}\sum_{n\mu}\int_k f_{n\mu}\big(2\partial_x G_{n\mu}^{yy} - \partial_y G_{n\mu}^{xy}\big), \tag{7}$$

where $G_{n\mu}^{ab} = \sum_{m\nu} g_{n\mu,m\nu}^{ab}/\varepsilon_{n\mu,m\nu}$ with $m \neq n$. The derived NHE expression is only for the quantum metric between non-degenerate bands ("inter-Kramers pairs"), and is consistent with Ref. [50]. The result can be also be viewed from the point of view of semiclassical theory. The origin of the NHE is traced to systematic corrections to the Berry curvature and energy dispersion stemming from the dressing of operators due to the electric field. Semiclassically, $H \to H + e\mathbf{E}\cdot\mathbf{r}$. Invoking the $U(1)^N$ symmetry of the block Hamiltonian, it is possible to remove the gauge-dependent linear coupling via a unitary transformation $H' = e^{-S}He^S$, with S fixed to remove the linear in $\mathbf{E}$ contribution (see Ref. [50]). However, it should be noted that the semiclassical approach fixes the diagonal components of H'. It is also possible to construct off-diagonal elements of H' and hence $v' = \frac{\partial H'}{\partial \mathbf{k}}$. By allowing off-diagonal elements in the Boltzmann equation away from the clean limit, one recovers Eqs. (4) and (5). Importantly, in the limit where the relaxation τ only enters the diagonal part of the density function $f_{n\mu}$ (the standard semiclassical assumption), the result of the Boltzmann treatment and the approach presented here coincide completely.

In PT-breaking systems, the asymmetric potential V_0 splits the energy of two spin bands within one Kramers pair. When the energy difference between these two spin bands is much larger than the disorder level, i.e., $V_0 \gg \Delta_\tau$, the relaxation time approximation [Eq. (6)] is valid for any pairs of (n, μ) and (m, ν) and thus $\alpha_{n\mu,m\nu} = \frac{2}{\varepsilon_{n\mu,m\nu}}$ and $\beta_{n\mu,m\nu} = -\frac{1}{\varepsilon_{n\mu,m\nu}}$ for both intra-Kramers pairs ($n = m$) and inter-Kramers pairs ($n \neq m$). We then obtain a similar expression as Eq. (7), but the summation over m in $G_{n\mu}^{ab} = \sum_{m\nu} g_{n\mu,m\nu}^{ab}/\varepsilon_{n\mu,m\nu}$ should also includes $m = n$. Therefore, the quantum metric within one Kramers pair of bands ("intra-Kramers pair") can also contribute to the NHE in addition to the inter-Kramers-pairs part.

IV. ELECTRIC FIELD CONTROL OF NHE

We numerically evaluate the NHE for the model Hamiltonian [Eq. (1)] based on Eq. (2). Figures 2(a) and 2(b) shows the Fermi energy ε_f dependence of the inter-Kramers-pair contribution $\sigma_{xyy}^{\text{inter}}$ and the intra-Kramers-pair contribution $\sigma_{xyy}^{\text{intra}}$ at different coupling coefficients t, respectively, at $V_0 = 2\,\text{meV}$, $\Gamma = 0.6\,\text{meV}$, and assuming the disorder level is very low ($V_0 \gg \hbar/\tau$). For both components, σ_{xyy} displays the same sign in the electron and hole doping regions. The intra-Kramers-pair contribution $\sigma_{xyy}^{\text{intra}}$ vanishes for $t = 0\,\text{meV}$, which indicates that the interlayer hybridization term is crucial for the nonzero quantum metric between two bands in one Kramers pair. Furthermore, $\sigma_{xyy}^{\text{intra}}$ increases with t while the inter-Kramers-pairs contribution $\sigma_{xyy}^{\text{inter}}$ decreases, as illustrated in Fig. 2(c), which plots the maximum values $\max(\sigma_{xyy}^{\text{intra}})$ and $\max(\sigma_{xyy}^{\text{inter}})$ as a function of t. Here, the maximum refers to the peak value of $\sigma_{xyy}^{\text{intra}}$ and $\sigma_{xyy}^{\text{inter}}$ when varying with ε_f in Figs. 2(a) and 2(b). Therefore, the intra-Kramers-pair contribution $\sigma_{xyy}^{\text{intra}}$ plays a more important role when the interlayer hybridization is stronger, i.e., when the sample thickness is thinner.

We summarize $\max(\sigma_{xyy})$ as a function of V_0 in Fig. 3(a), in which the green curve depicts the variation of total $\max(\sigma_{xyy})$, while the blue and red curves illustrate $\max(\sigma_{xyy}^{\text{intra}})$ and $\max(\sigma_{xyy}^{\text{inter}})$, respectively, at $t = 2\,\text{meV}$ and $\hbar/\tau = 0.5\,\text{meV}$. The intra-Kramers-pair contribution $\max(\sigma_{xyy}^{\text{intra}})$ is zero at $V_0 \sim 0$, and increases rapidly when V_0 is increasing. In contrast, the inter-Kramers-pairs contribution $\max(\sigma_{xyy}^{\text{inter}})$ almost remains constant with increasing V_0. Thus, one can divide the variation of $\max(\sigma_{xyy})$ into three regions for a fixed disorder strength. When $V_0 \ll \hbar/\tau$, $\max(\sigma_{xyy}^{\text{intra}})$ is close to zero and $\max(\sigma_{xyy}^{\text{inter}})$ dominates. When $V_0 \sim \hbar/\tau$, $\max(\sigma_{xyy}^{\text{intra}})$ increases rapidly with V_0, while $\max(\sigma_{xyy}^{\text{inter}})$ exhibits a small decrease.

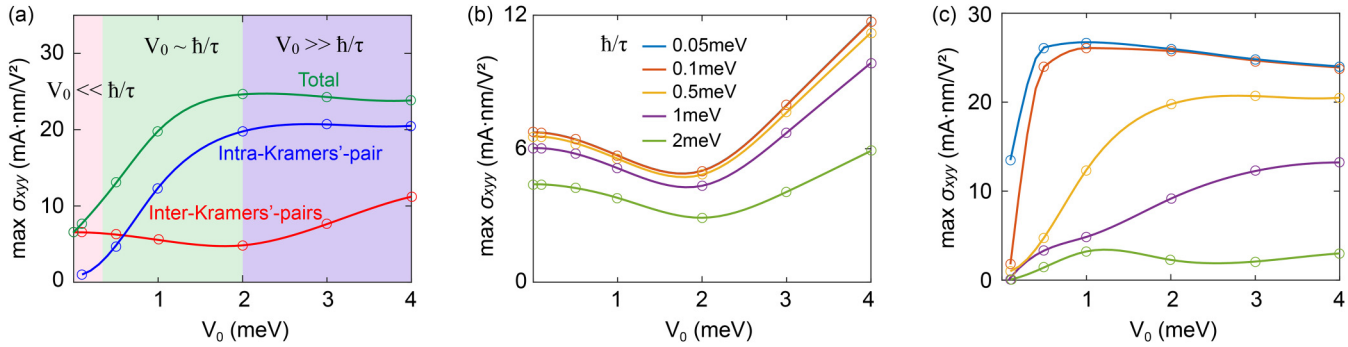

FIG. 3. (a) The maximum value of σ_{xyy} for the intra-Kramers-pair (blue), inter-Kramers-pairs (red), and total (green) contributions as a function of asymmetric potential V_0 at $t = 2$ meV and $\hbar/\tau = 0.5$ meV. (b) The maximum value of $\sigma_{xyy}^{\text{inter}}$ as a function of asymmetric potential V_0 at different disorder levels $\hbar/\tau$ for the inter-Kramers-pairs contribution at $t = 2$ meV. (c) The maximum value of $\sigma_{xyy}^{\text{intra}}$ as a function of V_0 for the intra-Kramers-pair contribution at $t = 2$ meV.

When $V_0 \gg \hbar/\tau$, $\max(\sigma_{xyy}^{\text{intra}})$ saturates while $\max(\sigma_{xyy}^{\text{inter}})$ reveals an upturn. Figures 3(b) and 3(c) show the $\max(\sigma_{xyy}^{\text{inter}})$ and $\max(\sigma_{xyy}^{\text{intra}})$ as a function of V_0 for different $\hbar/\tau$. The above scenario for the division of three regions generally remains valid for different $\hbar/\tau$ values. Furthermore, with increasing $\hbar/\tau$, both $\max(\sigma_{xyy}^{\text{inter}})$ and $\max(\sigma_{xyy}^{\text{intra}})$ are reduced.

V. CONCLUSION

To summarize, we showed the enhancement of the intrinsic NHE in AFM TI sandwiches via the breaking of inversion symmetry. The intrinsic NHE has been observed for even SLs of $MnBi_2Te_4$ in two recent experiments [55,56], and the displacement field dependence of the NHE has been measured. As discussed previously, the amount of enhancement is affected by the film thickness as well as the disorder level in the system. In Ref. [55], a small enhancement of the NHE was reported as the displacement field increases. The conductivity in this experiment is $\sigma_{xx} \approx 14$ mS at a carrier density $n_e = 3 \times 10^{12}$ cm^{-2}, and from $\tau = \frac{m^* \sigma_{xx}}{e^2 n_e}$ with the electron effective mass $m^* \approx 0.1 m_e$ [69], we estimate the disorder level to be $\hbar/\tau \sim 0.4$ meV. However, the experiment was perform in 6 SL $MnBi_2Te_4$, of which the hybridization strength between two surface states is considerably small [58–61], thus suppressing the intra-Kramers-pair contribution, as well as the enhancement of NHE. In Ref. [56], on the other hand, very little or no increase of the NHE was observed in the displacement field dependence measurement. We estimate the disorder level as $\hbar/\tau \sim 20$ meV with $\sigma_{xx}/n_e \approx 9 \times 10^{-11}$ μS cm^2 and strong disorder scattering can greatly suppress the NHE enhancement.

The scaling analysis between the nonlinear Hall conductivity and the longitudinal conductivity by varying temperatures has been used to distinguish the intrinsic NHE, which is the sole contribution that is independent of relaxation time τ in the weak disorder limit, from other extrinsic mechanisms, e.g., skew scattering and side jump [49,56,70–72], with strong dependence on τ. As our NHE formula Eq. (2) is beyond the weak disorder limit, the relaxation time τ dependence of the intrinsic NHE is found in Figs. 3(b) and 3(c), when the disorder broadening is comparable to band energy splitting. We note in both experiments [55,56] the NHE shows very little dependence of τ when varying temperatures. As the NHE only appears below the Néel temperature ∼24 K [73], we can estimate the change of relaxation time to be $\frac{\delta\tau}{\tau} \sim 20\%$ within this temperature range. From Figs. 3(b) and 3(c), a significant change of NHE can only occur when τ is changed several times. Thus, a 20% variation of τ can only give a negligible change of NHE, while more feasible control is through a displacement field [55].

In our calculations, the value of NHE is around the order of 10 mA nm/V^2, while the experimental values reported in Refs. [55,56] are both ∼100 mA nm/V^2, one order larger than the calculated value. To explain this discrepancy, it was proposed that the quantum metric in experiments might be enhanced by the modified surface band structure of $MnBi_2Te_4$ [56]. As disorder scattering is strong in Ref. [56], a full quantum mechanical treatment of the disorder effect beyond the relaxation time approximation [70,71,74,75] is required. Furthermore, the edge transport may also give rise to the NHE for the Fermi energy close to the band edges [76,77], which is beyond the current theoretical formalism.

ACKNOWLEDGMENTS

We thank Weibo Gao for helpful discussion. R.M., C.-Z.C., and C.-X.L. acknowledge the support from the NSF through The Pennsylvania State University Materials Research Science and Engineering Center (DMR-2011839). C.-Z.C. and C.-X.L. also acknowledge support from NSF Grant No. DMR-2241327. C.-Z.C. acknowledges the support from the Gordon and Betty Moore Foundation's EPiQS Initiative (Grant No. GBMF9063 to C.-Z.C.). D.K. is supported by the Abrahams Postdoctoral Fellowship of the Center for Materials Theory, Rutgers University, and the Zuckerman STEM Fellowship. B.Y. acknowledges the financial support by the European Research Council (ERC Consolidator Grant "NonlinearTopo," No. 815869) and the Israel Science Foundation (ISF: 2932/21, 2974/23).

[1] X.-L. Qi, T. L. Hughes, and S.-C. Zhang, Topological field theory of time-reversal invariant insulators, Phys. Rev. B **78**, 195424 (2008).

[2] R. Yu, W. Zhang, H.-J. Zhang, S.-C. Zhang, X. Dai, and Z. Fang, Quantized anomalous Hall effect in magnetic topological insulators, Science **329**, 61 (2010).

[3] C.-Z. Chang, J. Zhang, X. Feng, J. Shen, Z. Zhang, M. Guo, K. Li, Y. Ou, P. Wei, L.-L. Wang *et al.*, Experimental observation of the quantum anomalous Hall effect in a magnetic topological insulator, Science **340**, 167 (2013).

[4] C.-Z. Chang, W. Zhao, D. Y. Kim, H. Zhang, B. A. Assaf, D. Heiman, S.-C. Zhang, C. Liu, M. H. Chan, and J. S. Moodera, High-precision realization of robust quantum anomalous Hall state in a hard ferromagnetic topological insulator, Nat. Mater. **14**, 473 (2015).

[5] M. Mogi, R. Yoshimi, A. Tsukazaki, K. Yasuda, Y. Kozuka, K. Takahashi, M. Kawasaki, and Y. Tokura, Magnetic modulation doping in topological insulators toward higher-temperature quantum anomalous Hall effect, Appl. Phys. Lett. **107**, 182401 (2015).

[6] Y. Ou, C. Liu, G. Jiang, Y. Feng, D. Zhao, W. Wu, X.-X. Wang, W. Li, C. Song, L.-L. Wang *et al.*, Enhancing the quantum anomalous Hall effect by magnetic codoping in a topological insulator, Adv. Mater. **30**, 1703062 (2018).

[7] Y. Deng, Y. Yu, M. Z. Shi, Z. Guo, Z. Xu, J. Wang, X. H. Chen, and Y. Zhang, Quantum anomalous Hall effect in intrinsic magnetic topological insulator $MnBi_2Te_4$, Science **367**, 895 (2020).

[8] C.-Z. Chang, C.-X. Liu, and A. H. MacDonald, *Colloquium*: Quantum anomalous Hall effect, Rev. Mod. Phys. **95**, 011002 (2023).

[9] X. Kou, L. Pan, J. Wang, Y. Fan, E. S. Choi, W.-L. Lee, T. Nie, K. Murata, Q. Shao, S.-C. Zhang *et al.*, Metal-to-insulator switching in quantum anomalous Hall states, Nat. Commun. **6**, 8474 (2015).

[10] J. Wang, B. Lian, and S.-C. Zhang, Universal scaling of the quantum anomalous Hall plateau transition, Phys. Rev. B **89**, 085106 (2014).

[11] D. Xiao, J. Jiang, J.-H. Shin, W. Wang, F. Wang, Y.-F. Zhao, C. Liu, W. Wu, M. H. Chan, N. Samarth, and C. Z. Chang, Realization of the axion insulator state in quantum anomalous Hall sandwich heterostructures, Phys. Rev. Lett. **120**, 056801 (2018).

[12] M. Mogi, M. Kawamura, A. Tsukazaki, R. Yoshimi, K. S. Takahashi, M. Kawasaki, and Y. Tokura, Tailoring tricolor structure of magnetic topological insulator for robust axion insulator, Sci. Adv. **3**, eaao1669 (2017).

[13] X.-L. Qi and S.-C. Zhang, Topological insulators and superconductors, Rev. Mod. Phys. **83**, 1057 (2011).

[14] R.-L. Chu, J. Shi, and S.-Q. Shen, Surface edge state and half-quantized Hall conductance in topological insulators, Phys. Rev. B **84**, 085312 (2011).

[15] A. L. Sharpe, E. J. Fox, A. W. Barnard, J. Finney, K. Watanabe, T. Taniguchi, M. Kastner, and D. Goldhaber-Gordon, Emergent ferromagnetism near three-quarters filling in twisted bilayer graphene, Science **365**, 605 (2019).

[16] M. Serlin, C. Tschirhart, H. Polshyn, Y. Zhang, J. Zhu, K. Watanabe, T. Taniguchi, L. Balents, and A. Young, Intrinsic quantized anomalous Hall effect in a moiré heterostructure, Science **367**, 900 (2020).

[17] F. Xu, Z. Sun, T. Jia, C. Liu, C. Xu, C. Li, Y. Gu, K. Watanabe, T. Taniguchi, B. Tong *et al.*, Observation of integer and fractional quantum anomalous Hall effects in twisted bilayer $MoTe_2$, Phys. Rev. X **13**, 031037 (2023).

[18] J. Cai, E. Anderson, C. Wang, X. Zhang, X. Liu, W. Holtzmann, Y. Zhang, F. Fan, T. Taniguchi, K. Watanabe *et al.*, Signatures of fractional quantum anomalous Hall states in twisted $MoTe_2$, Nature (London) **622**, 63 (2023).

[19] Z. Lu, T. Han, Y. Yao, A. P. Reddy, J. Yang, J. Seo, K. Watanabe, T. Taniguchi, L. Fu, and L. Ju, Fractional quantum anomalous Hall effect in multilayer graphene, Nature (London) **626**, 759 (2024).

[20] H. Park, J. Cai, E. Anderson, Y. Zhang, J. Zhu, X. Liu, C. Wang, W. Holtzmann, C. Hu, Z. Liu *et al.*, Observation of fractionally quantized anomalous Hall effect, Nature (London) **622**, 74 (2023).

[21] Z. Tao, B. Shen, S. Jiang, T. Li, L. Li, L. Ma, W. Zhao, J. Hu, K. Pistunova, K. Watanabe *et al.*, Valley-coherent quantum anomalous Hall state in AB-stacked $MoTe_2/WSe_2$ bilayers, Phys. Rev. X **14**, 011004 (2024).

[22] T. Han, Z. Lu, G. Scuri, J. Sung, J. Wang, T. Han, K. Watanabe, T. Taniguchi, H. Park, and L. Ju, Correlated insulator and Chern insulators in pentalayer rhombohedral-stacked graphene, Nat. Nanotechnol. **19**, 181 (2024).

[23] T. Han, Z. Lu, Y. Yao, J. Yang, J. Seo, C. Yoon, K. Watanabe, T. Taniguchi, L. Fu, F. Zhang *et al.*, Large quantum anomalous Hall effect in spin-orbit proximitized rhombohedral graphene, Science **384**, 647 (2024).

[24] Y. Sha, J. Zheng, K. Liu, H. Du, K. Watanabe, T. Taniguchi, J. Jia, Z. Shi, R. Zhong, and G. Chen, Observation of a Chern insulator in crystalline ABCA-tetralayer graphene with spin-orbit coupling, Science **384**, 414 (2024).

[25] M. M. Otrokov, I. I. Klimovskikh, H. Bentmann, D. Estyunin, A. Zeugner, Z. S. Aliev, S. Gaß, A. Wolter, A. Koroleva, A. M. Shikin *et al.*, Prediction and observation of an antiferromagnetic topological insulator, Nature (London) **576**, 416 (2019).

[26] Y. Gong, J. Guo, J. Li, K. Zhu, M. Liao, X. Liu, Q. Zhang, L. Gu, L. Tang, X. Feng *et al.*, Experimental realization of an intrinsic magnetic topological insulator, Chin. Phys. Lett. **36**, 076801 (2019).

[27] J. Li, Y. Li, S. Du, Z. Wang, B.-L. Gu, S.-C. Zhang, K. He, W. Duan, and Y. Xu, Intrinsic magnetic topological insulators in van der Waals layered $MnBi_2Te_4$-family materials, Sci. Adv. **5**, eaaw5685 (2019).

[28] D. Zhang, M. Shi, T. Zhu, D. Xing, H. Zhang, and J. Wang, Topological axion states in the magnetic insulator $MnBi_2Te_4$ with the quantized magnetoelectric effect, Phys. Rev. Lett. **122**, 206401 (2019).

[29] Y.-H. Li and R. Cheng, Identifying axion insulator by quantized magnetoelectric effect in antiferromagnetic $MnBi_2Te_4$ tunnel junction, Phys. Rev. Res. **4**, L022067 (2022).

[30] L. Wu, M. Salehi, N. Koirala, J. Moon, S. Oh, and N. Armitage, Quantized Faraday and Kerr rotation and axion electrodynamics of a 3D topological insulator, Science **354**, 1124 (2016).

[31] V. Dziom, A. Shuvaev, A. Pimenov, G. Astakhov, C. Ames, K. Bendias, J. Böttcher, G. Tkachov, E. Hankiewicz, C. Brüne *et al.*, Observation of the universal magnetoelectric effect in a 3D topological insulator, Nat. Commun. **8**, 15197 (2017).

[32] K. N. Okada, Y. Takahashi, M. Mogi, R. Yoshimi, A. Tsukazaki, K. S. Takahashi, N. Ogawa, M. Kawasaki, and Y. Tokura,

Terahertz spectroscopy on Faraday and Kerr rotations in a quantum anomalous Hall state, Nat. Commun. **7**, 12245 (2016).
[33] W.-K. Tse and A. H. MacDonald, Giant magneto-optical Kerr effect and universal Faraday effect in thin-film topological insulators, Phys. Rev. Lett. **105**, 057401 (2010).
[34] A. Sekine and K. Nomura, Axion electrodynamics in topological materials, J. Appl. Phys. **129**, 141101 (2021).
[35] T. Holder, D. Kaplan, and B. Yan, Consequences of time-reversal-symmetry breaking in the light-matter interaction: Berry curvature, quantum metric, and diabatic motion, Phys. Rev. Res. **2**, 033100 (2020).
[36] Q. Ma, A. G. Grushin, and K. S. Burch, Topology and geometry under the nonlinear electromagnetic spotlight, Nat. Mater. **20**, 1601 (2021).
[37] F. de Juan, A. G. Grushin, T. Morimoto, and J. E. Moore, Quantized circular photogalvanic effect in Weyl semimetals, Nat. Commun. **8**, 15995 (2017).
[38] Y. Tokura and N. Nagaosa, Nonreciprocal responses from non-centrosymmetric quantum materials, Nat. Commun. **9**, 3740 (2018).
[39] T. Morimoto and N. Nagaosa, Topological nature of nonlinear optical effects in solids, Sci. Adv. **2**, e1501524 (2016).
[40] J. Orenstein, J. Moore, T. Morimoto, D. Torchinsky, J. Harter, and D. Hsieh, Topology and symmetry of quantum materials via nonlinear optical responses, Annu. Rev. Condens. Matter Phys. **12**, 247 (2021).
[41] Z. Du, H.-Z. Lu, and X. Xie, Nonlinear Hall effects, Nat. Rev. Phys. **3**, 744 (2021).
[42] J. W. Zuber and C. Zhang, Nonlinear effects in topological materials, Front. Optoelectron. **14**, 99 (2021).
[43] C. Bao, P. Tang, D. Sun, and S. Zhou, Light-induced emergent phenomena in 2D materials and topological materials, Nat. Rev. Phys. **4**, 33 (2022).
[44] N. Nagaosa and Y. Yanase, Nonreciprocal transport and optical phenomena in quantum materials, Annu. Rev. Condens. Matter Phys. **15**, 63 (2023).
[45] I. Sodemann and L. Fu, Quantum nonlinear Hall effect induced by Berry curvature dipole in time-reversal invariant materials, Phys. Rev. Lett. **115**, 216806 (2015).
[46] Y. Zhang, Y. Sun, and B. Yan, Berry curvature dipole in Weyl semimetal materials: An *ab initio* study, Phys. Rev. B **97**, 041101(R) (2018).
[47] Q. Ma, S.-Y. Xu, H. Shen, D. MacNeill, V. Fatemi, T.-R. Chang, A. M. Mier Valdivia, S. Wu, Z. Du, C.-H. Hsu *et al.*, Observation of the nonlinear Hall effect under time-reversal-symmetric conditions, Nature (London) **565**, 337 (2019).
[48] Z. Z. Du, C. M. Wang, H.-Z. Lu, and X. C. Xie, Band signatures for strong nonlinear Hall effect in bilayer WTe_2, Phys. Rev. Lett. **121**, 266601 (2018).
[49] C. Wang, Y. Gao, and D. Xiao, Intrinsic nonlinear Hall effect in antiferromagnetic tetragonal CuMnAs, Phys. Rev. Lett. **127**, 277201 (2021).
[50] D. Kaplan, T. Holder, and B. Yan, Unification of nonlinear anomalous Hall effect and nonreciprocal magnetoresistance in metals by the quantum geometry, Phys. Rev. Lett. **132**, 026301 (2024).
[51] Y. Gao, S. A. Yang, and Q. Niu, Field induced positional shift of Bloch electrons and its dynamical implications, Phys. Rev. Lett. **112**, 166601 (2014).
[52] H. Liu, J. Zhao, Y.-X. Huang, W. Wu, X.-L. Sheng, C. Xiao, and S. A. Yang, Intrinsic second-order anomalous Hall effect and its application in compensated antiferromagnets, Phys. Rev. Lett. **127**, 277202 (2021).
[53] J. Ahn, S. Park, and B.-J. Yang, Failure of Nielsen-Ninomiya theorem and fragile topology in two-dimensional systems with space-time inversion symmetry: Application to twisted bilayer graphene at magic angle, Phys. Rev. X **9**, 021013 (2019).
[54] H. Tasaki, *Physics and Mathematics of Quantum Many-Body Systems* (Springer, Berlin, 2020), Vol. 66.
[55] A. Gao, Y.-F. Liu, J.-X. Qiu, B. Ghosh, T. V. Trevisan, Y. Onishi, C. Hu, T. Qian, H.-J. Tien, S.-W. Chen *et al.*, Quantum metric nonlinear Hall effect in a topological antiferromagnetic heterostructure, Science **381**, 181 (2023).
[56] N. Wang, D. Kaplan, Z. Zhang, T. Holder, N. Cao, A. Wang, X. Zhou, F. Zhou, Z. Jiang, C. Zhang *et al.*, Quantum-metric-induced nonlinear transport in a topological antiferromagnet, Nature (London) **621**, 487 (2023).
[57] L. Fu, Hexagonal warping effects in the surface states of the topological insulator Bi_2Te_3, Phys. Rev. Lett. **103**, 266801 (2009).
[58] Y. Zhang, K. He, C.-Z. Chang, C.-L. Song, L.-L. Wang, X. Chen, J.-F. Jia, Z. Fang, X. Dai, W.-Y. Shan *et al.*, Crossover of the three-dimensional topological insulator Bi_2Se_3 to the two-dimensional limit, Nat. Phys. **6**, 584 (2010).
[59] Y. Sakamoto, T. Hirahara, H. Miyazaki, S.-I. Kimura, and S. Hasegawa, Spectroscopic evidence of a topological quantum phase transition in ultrathin Bi_2Se_3 films, Phys. Rev. B **81**, 165432 (2010).
[60] Z. Wang, T. Zhou, T. Jiang, H. Sun, Y. Zang, Y. Gong, J. Zhang, M. Tong, X. Xie, Q. Liu *et al.*, Dimensional crossover and topological nature of the thin films of a three-dimensional topological insulator by band gap engineering, Nano Lett. **19**, 4627 (2019).
[61] M. Fang, Z. Wang, H. Gu, M. Tong, B. Song, X. Xie, T. Zhou, X. Chen, H. Jiang, T. Jiang *et al.*, Layer-dependent dielectric permittivity of topological insulator Bi_2Se_3 thin films, Appl. Surf. Sci. **509**, 144822 (2020).
[62] See Supplemental Material at http://link.aps.org/supplemental/10.1103/PhysRevB.110.165401 for detailed derivations of the nonlinear Hall effect, symmetry analysis of nonlinear conductivity, and Fermi sphere contribution to the nonlinear Hall conductivity, which also includes Refs. [63–67].
[63] D. Kaplan, T. Holder, and B. Yan, General nonlinear Hall current in magnetic insulators beyond the quantum anomalous Hall effect, Nat. Commun. **14**, 3053 (2023).
[64] F. G. Utermohlen and N. Trivedi, Symmetry analysis of tensors in the honeycomb lattice of edge-sharing octahedra, Phys. Rev. B **103**, 155124 (2021).
[65] D. J. Passos, G. B. Ventura, J. M. Viana Parente Lopes, J. M. B. Lopes dos Santos, and N. M. R. Peres, Nonlinear optical responses of crystalline systems: Results from a velocity gauge analysis, Phys. Rev. B **97**, 235446 (2018).
[66] D. Ma, A. Arora, G. Vignale, and J. C. W. Song, Anomalous skew-scattering nonlinear Hall effect and chiral photocurrents in PT-symmetric antiferromagnets, Phys. Rev. Lett. **131**, 076601 (2023).
[67] H. Watanabe and Y. Yanase, Nonlinear electric transport in odd-parity magnetic multipole systems: Application to Mn-based compounds, Phys. Rev. Res. **2**, 043081 (2020).

[68] M.-T. Suzuki, T. Koretsune, M. Ochi, and R. Arita, Cluster multipole theory for anomalous Hall effect in antiferromagnets, Phys. Rev. B **95**, 094406 (2017).

[69] Y. An, K. Wang, S. Gong, Y. Hou, C. Ma, M. Zhu, C. Zhao, T. Wang, S. Ma, H. Wang *et al.*, Nanodevices engineering and spin transport properties of $MnBi_2Te_4$ monolayer, npj Comput. Mater. **7**, 45 (2021).

[70] Z. Du, C. Wang, S. Li, H.-Z. Lu, and X. Xie, Disorder-induced nonlinear Hall effect with time-reversal symmetry, Nat. Commun. **10**, 3047 (2019).

[71] S. Nandy and I. Sodemann, Symmetry and quantum kinetics of the nonlinear Hall effect, Phys. Rev. B **100**, 195117 (2019).

[72] Z. Du, C. Wang, H.-P. Sun, H.-Z. Lu, and X. Xie, Quantum theory of the nonlinear Hall effect, Nat. Commun. **12**, 5038 (2021).

[73] K. He, $MnBi_2Te_4$-family intrinsic magnetic topological materials, npj Quantum Mater. **5**, 90 (2020).

[74] C. Xiao, Z. Z. Du, and Q. Niu, Theory of nonlinear Hall effects: Modified semiclassics from quantum kinetics, Phys. Rev. B **100**, 165422 (2019).

[75] C. Ortix, Nonlinear Hall effect with time-reversal symmetry: Theory and material realizations, Adv. Quantum Technol. **4**, 2100056 (2021).

[76] K. Yasuda, T. Morimoto, R. Yoshimi, M. Mogi, A. Tsukazaki, M. Kawamura, K. S. Takahashi, M. Kawasaki, N. Nagaosa, and Y. Tokura, Large non-reciprocal charge transport mediated by quantum anomalous Hall edge states, Nat. Nanotechnol. **15**, 831 (2020).

[77] Z. Zhang, N. Wang, N. Cao, A. Wang, X. Zhou, K. Watanabe, T. Taniguchi, B. Yan, and W.-B. Gao, Controlled large non-reciprocal charge transport in an intrinsic magnetic topological insulator $MnBi_2Te_4$, Nat. Commun. **13**, 6191 (2022).